Journal of Geophysical Research: Space Physics

RESEARCH ARTICLE
10.1029/2018JA025796

Plasmaspheric Plumes and EMIC Rising Tone Emissions

B. Grison[1], M. Hanzelka[1,4], H. Breuillard[2], F. Darrouzet[3], O. Santolík[1,4], N. Cornilleau-Wehrlin[2], and I. Dandouras[5]

[1]Department of Space Physics, Institute of Atmospheric Physics, The Czech Academy of Sciences, Prague, Czech Republic , [2]Laboratoire de Physique des Plasmas, CNRS/Ecole Polytechnique/Obs. de Paris/UPMC/Univ. Paris-Sud, Palaiseau, France, [3]Royal Belgian Institute for Space Aeronomy, Brussels, Belgium, [4]Faculty of Mathematics and Physics, Charles University, Prague, Czech Republic, [5]Institut de Recherche en Astrophysique et Planétologie, University of Toulouse/CNRS/UPS/CNES, Toulouse, France

Key Points:
- Coherent rising tones are found in 20% (6/30) of the plume (and vicinity) events with EMIC emissions
- EMIC rising tones are observed at magnetic latitudes larger than 17 degrees and up to 35 degrees
- Emissions below H^+ gyrofrequency in the vicinity of plasmaspheric plumes are mainly broadband

Correspondence to:
B. Grison,
grison@ufa.cas.cz

Citation:
Grison, B., Hanzelka, M., Breuillard, H., Darrouzet, F., Santolík, O., Cornilleau-Wehrlin, N., & Dandouras, I. (2018). Plasmaspheric plumes and EMIC rising tone emissions. *Journal of Geophysical Research: Space Physics*, *123*, 9443–9452. https://doi.org/10.1029/2018JA025796

Received 18 JUN 2018
Accepted 29 OCT 2018
Accepted article online 10 NOV 2018
Published online 28 NOV 2018

Abstract Due to its polar orbit Cluster spacecraft crossed plasmaspheric plumes out of the magnetic equatorial plane. We study the occurrence of broadband, narrowband, and rising tone emissions in the plume vicinity, below the local proton gyrofrequency. Based on a database of 935 Cluster plumes crossings, reduced to 189 unique plumes, we find that broadband activity is the most common case. We confirm result from a previous study showing that plume vicinity is not a preferred place for observing narrowband emissions. Rising tones are the less frequently observed of these three kinds of emissions. Nevertheless, ElectroMagnetic Ion Cyclotron (EMIC) rising tone occurrence rate is high compared to the narrowband one: Tones are seen in six of 30 plume events (20%) when narrowband emissions are observed. Rising tones are observed at absolute magnetic latitudes larger than 17° and up to 35° . We detail the 16 August 2005 plume crossing when a rising tone is observed. Results of a ray tracing analysis agree with a tone triggering process taking place above 15° of magnetic latitude.

1. Introduction

Depending on the background magnetic field ($\mathbf{B}_0$) intensity and the plasmasphere extent, local proton gyrofrequency (f_{H+}) at the Earth's plasmapause typically varies between 1 and 10 Hz. ElectroMagnetic Ion Cyclotron (EMIC) waves are narrowband emissions observed below f_{H^+}. The free energy for EMIC wave growth mainly results from proton temperature anisotropy (Kennel & Petschek, 1966), and the wave growth maximizes in region of minima of $\mathbf{B}_0$ and/or of density increase. EMIC emissions are observed in various part of the magnetosphere, including the plasmapause region (e.g., Anderson et al., 1992; Usanova et al., 2012).

When EMIC linear amplification saturates, nonlinear process starts and sub-wave packets of increasing frequencies forming rising tones can be observed (Omura et al., 2010). The frequency with time dispersion (sweep rate) is a key feature for in situ tone identification (Pickett et al., 2010). These emissions are usually referred to as EMIC-triggered emissions (referring to generation mechanism) or EMIC rising tones (referring to observational shape). As the triggering process is not the core of this study, we use EMIC rising tone name in what follows. Another key parameter for identification is the tone emission coherence level, which is higher than the surrounding narrowband EMIC waves one (Grison et al., 2013).

Plasmaspheric plumes are plasma regions partially detached from plasmasphere consecutive to geomagnetic storms or substorms (e.g., Elphic et al., 1996; Darrouzet et al., 2009). Plasma density gradients observed in the plumes do not make plumes a preferred region for EMIC wave observations (Usanova et al., 2013). Due to the Cluster (Escoubet et al., 2001) polar orbit and its perigee inside the plasmasphere, Cluster spacecraft cross plumes off the magnetic equatorial plane, where EMIC rising tones have not been reported yet. In this paper we compare the occurrence rate of broadband, narrowband, and rising tone emissions, below f_{H^+} and in the vicinity of plasmaspheric plumes crossed by Cluster.

After presenting the instrumentation, the methodology, and the occurrence rate of these three types of emissions (section 2), we detail wave and particle observations and ray tracing analysis of a plume crossing with rising tone to infer the tone triggering place (section 3). We discuss (section 4) our results before concluding (section 5).

Table 1
Number of Individual Crossings of a Given Plasmaspheric Plume by All the Cluster Spacecraft

	1x	2x	3x	4x	5x	6x	7x	8x	Total
1. Hemisphere	12	11	13	**31**	—	—	—	—	67
2. Hemispheres	—	12	6	13	9	23	11	**48**	122

Note. Dashes stand for nonapplicable, and largest subset number in each row is in bold.

2. Statistical Study

2.1. Instrumentation

Each of the four spacecraft of the Cluster mission contains 11 identical instruments (Escoubet et al., 2001). The flux gate magnetometer (FGM) data are used for $\mathbf{B}_0$ measurements and for the magnetic field fluctuation ($\mathbf{B}$) measurements (Balogh et al., 2001). In addition to FGM, for the wave analysis we use Spatio Temporal Analysis of Field Fluctuations (STAFF) experiment waveform data, hereafter called STAFF-SC (Cornilleau-Wehrlin et al., 2003). STAFF response is better than the FGM one above 1 Hz and vice versa (Nykyri et al., 2006; Robert et al., 2014). Both FGM and STAFF-SC instruments can be used for EMIC emission study in the inner magnetosphere region. Electric field fluctuations ($\mathbf{E}$) are measured in the spacecraft spin plane by two electric antennas (Electric Field and Wave (EFW); Gustafsson et al., 2001). The plasma density is obtained from the Waves of High frequency and Sounder for Probing of Electron density by Relaxation (WHISPER) relaxation sounder measurements of the plasma frequency (Décréau et al., 2001), when in its range of operation (2–80 kHz), or from the spacecraft potential measured by EFW. Ion energy fluxes are studied with the Cluster Ion Spectrometry/Hot Ion Analyser (CIS/HIA) ion energy spectrometer and CIS/COmposition and DIstribution Function analyser (CIS/CODIF) ion mass spectrometer, which provides ion 3-D distributions separately for each of the main species (H^+, He^+, He^{2+}, and O^+; Rème et al., 2001).

2.2. Methodology

We consider a list of 993 plasmaspheric plume crossings by Cluster spacecraft from 1 February 2001 to 1 February 2006 (the 782 cases identified in Darrouzet et al., 2008, extended to the end of year 2006; Usanova et al., 2013). A plume is identified by a density increase of at least 10 cm^{-3} and a L-width of at least 0.2 Earth radii (R_E; cf. Darrouzet et al., 2008, pp. 2405–2406, for more details). A single plasmaspheric plume can be crossed in a single hemisphere at least once or in both hemispheres at least twice. There is no case with a spacecraft crossing the magnetic equator inside a plume. There is at most eight crossings of the same plasmaspheric plume: two crossings per spacecraft, one in each hemisphere. The individual 935 plume crossings with available STAFF-SC data can be then reduced to 189 unique plumes. Unique identifiers CXXX and PYYY, where XXX and YYY are three digit numbers, are given to each crossing and each plume. Table 1 details the number of individual crossings of a given plasmaspheric plume. In the most frequent case, the four Cluster spacecraft observe the same plume in a single hemisphere (31 plumes) or in both hemispheres (48 plumes): In the 2001-2006 years period, the spacecraft were nearly always in a close configuration.

For each crossing we report the maximum level of magnetic wave activity (PSD_{max}). Power spectral density (PSD) is computed on 512-point windows (about 20 s). There is a 480-point overlap between two consecutive windows. Emissions are classified as absent or weak (W), for $PSD_{max} < 10^{-3}$ $nT^2 \cdot Hz^{-1}$, and medium (M), for $PSD_{max} \geq 10^{-3}$ $nT^2 \cdot Hz^{-1}$. This is done separately for each type of waves, that is, broadband, narrowband, or rising tone emissions, based on a visual inspection of spectra. Broadband emissions start from the lowest accessible frequency and span over local proton and/or helium gyrofrequencies, while frequency range of narrowband emissions is limited.

We show examples of this classification in Figures 1 and 2 for two plume crossings. Top panels present the frequency versus time diagram (spectrogram) of the electric field measured by the WHISPER instrument. The electron plasma frequency (f_{pe}) is identified by intense electrostatic emissions. The plume start and end times are characterized by abrupt f_{pe} increase and decrease. Middle panels present the spectrogram of the total magnetic PSD (STAFF-SC instrument). Bottom panels present the wave ellipticity with a threshold of $10^{-3} \cdot Hz^{-1}$: It therefore appears only when the wave activity is M. The two vertical lines in the middle panel bound the plume proper. To compare our results with Usanova et al. (2013), we extend the observation time by 30 min before and after the plume crossing. On each panel local gyrofrequencies are overplotted in black (f_{H^+}) and red (f_{He^+}). Universal time (UT) and spacecraft position, in magnetic latitude (MLAT), magnetic local time (MLT), and radial distance in Earth radii (R_E), are indicated below the panels.

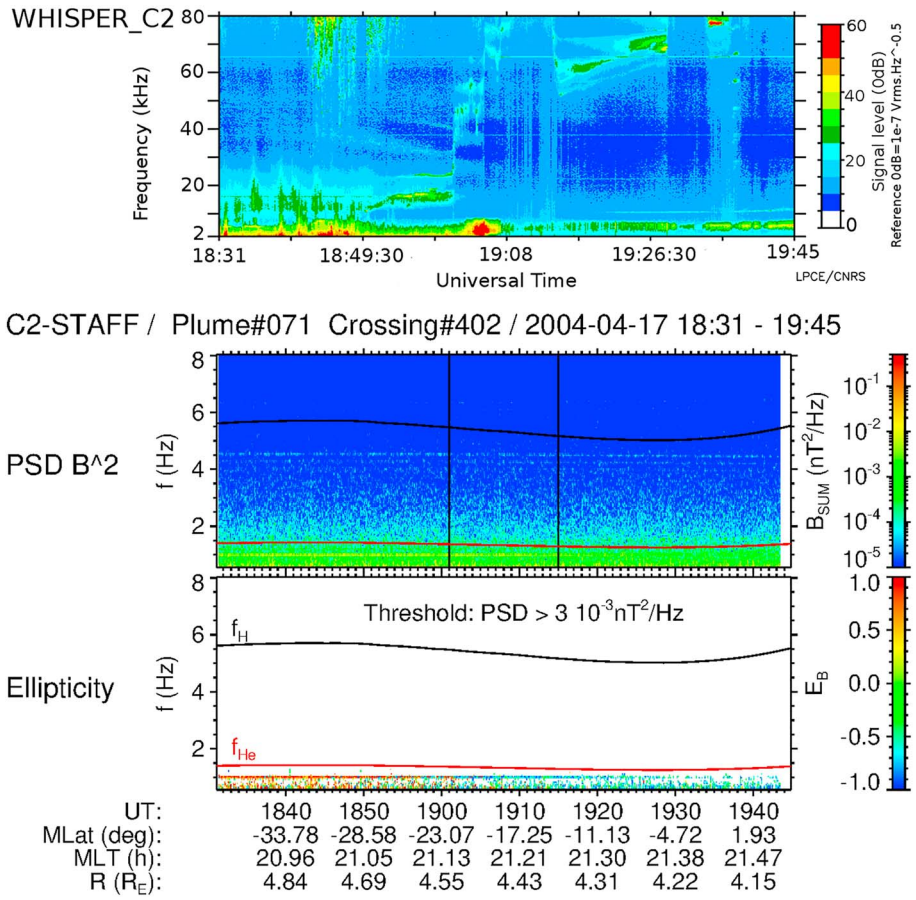

Figure 1. Example of plume crossings (1/2). Top (Waves of High frequency and Sounder for Probing of Electron density by Relaxation [WHISPER] instrument): Time-frequency electric field spectrogram, which shows the plasma frequency, giving evidence of the plume crossing. Middle (STAFF-SC instrument): total magnetic power spectral density (PSD) in $nT^2 \cdot Hz^{-1}$, two vertical black lines delimit the plume that is seen above on WHISPER data. Bottom panel (STAFF-SC instrument): wave ellipticity for emissions with a PSD larger than 10^{-3} $nT^2 \cdot Hz^{-1}$. Proton and He^+ local gyrofrequencies are plotted in black and red solid lines, respectively. Note that the frequency scale is in kHz in top panel and in Hz in middle and bottom panels.

In Figure 1 (C402, P071) one can see a typical crossing with no wave activity. The wave activity is set to W for the three types of emissions for this crossing. Medium broadband emissions are recorded during one (C405, not shown) of the eight P071 plume crossings by the four spacecraft. Plume P071 wave activity is therefore set to W intensity for the narrowband category and to M intensity for the broadband and overall categories.

In Figure 2 (C712, P122), broadband emissions are observed before and inside the plume. Narrowband emissions are observed after the plume crossing. For C712, both broadband and narrowband wave activities are considered in our study as M intensity. Plume P122 wave activity is also set to M intensity for narrowband and broadband categories.

2.3. Occurrence Rate of Broadband, Narrowband, and Rising Tone Emissions

The results obtained over 189 plumes (and 935 crossings) are summarized in Table 2. In 70% of the plume events (133/189) there is a noticeable PSD enhancement. The average number of individual plume crossings (4.1) is slightly lower in the W category case compared to the M category (5.3 crossings): The greater the number of spacecraft crossing of a given plume, the higher the probability to observe waves.

Broadband PSD enhancements of M intensity are the most common emissions: They are observed in two thirds of the plumes (127/189) and in 44 % of the individual crossings (416/935). Such enhancements are present in 62 % of individual crossings (416/671) in the 127 plumes with broadband emissions. Broadband activity is common in or close to the plasmaspheric plumes, and it is persistent on the time and/or space scale of the plume encounter by the Cluster spacecraft.

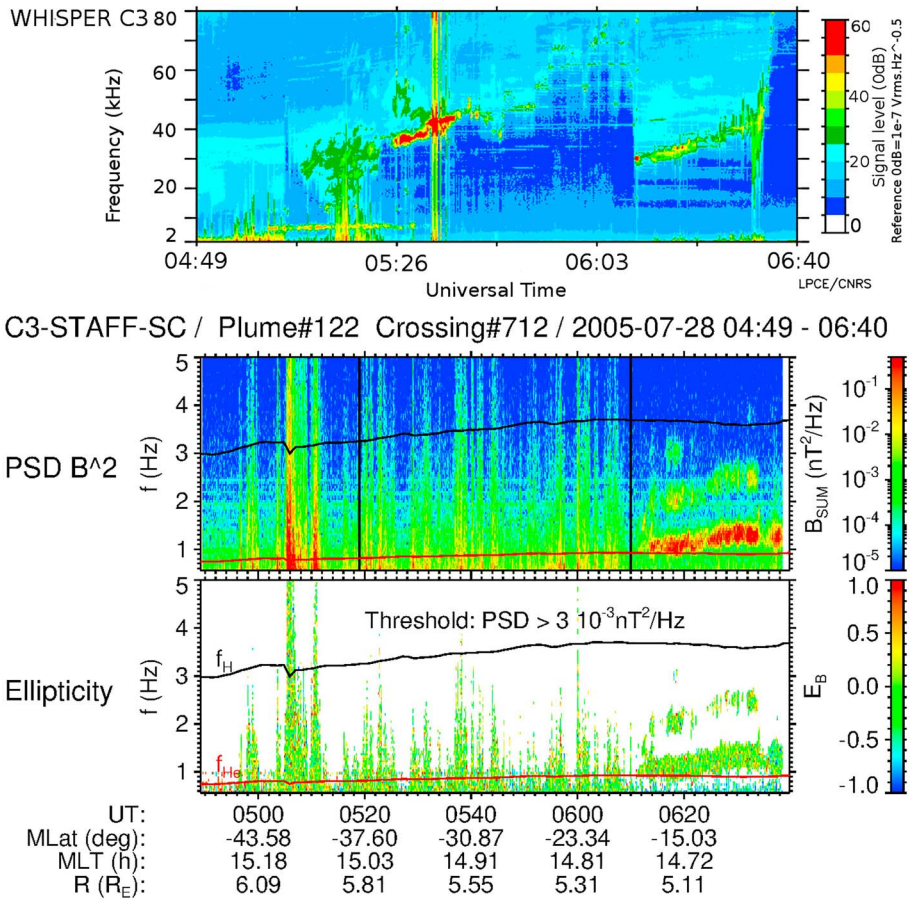

Figure 2. Example of plume crossings (2/2). See Figure 1 for panel description.

Narrowband emissions are observed in the vicinity of or in 30 plumes (16 % of the 189 plumes) and in 6 % of individual crossings (60/935). This is lower than 14 % found by Usanova et al. (2013) as discussed in section 4. Narrowband activity is observed in 34 % of individual crossings (60/175) in the 30 plumes with narrowband emissions. Narrowband emissions are probably related to more localized processes than the broadband emissions. Narrowband emissions are observed together with broadband activity in six plumes. There is no correlation between broadband and narrowband activities.

For each of the 60 individual crossings with narrow band emissions the presence of rising tones is investigated. Rising tones are identified by both frequency with time dispersion *and* enhanced coherence value. Only tones

Table 2
Magnetic Power Spectral Density Intensification Observed in the Vicinity of Plasmaspheric Plumes

	All		M-intensity emissions		
	W	M	Broad	Narrow	Tones
Plumes	56	133	127	30	6
Plumes (combined crossings)	231	704	671	175	28
M-intensity crossings	—	444	416	60	9
Crossings / Plumes	4.1	5.3	5.3	5.8	4.7
Hemisphere / Plumes	1.5	1.7	1.7	1.8	1.5

Note. W means no or weak activity ($PSD_{max} < 10^{-3}$ nT^2·Hz^{-1}); M means medium activity ($PSD_{max} \geq 10^{-3}$ nT^2·Hz^{-1}); tones means rising tones. The total number of crossings, with or without emissions, (see Table 1) of the various *plumes* subset is given in "Plumes (combined crossings)."

Table 3
Location of Rising Tone Observations (One Location per Spacecraft per Hemisphere)

Plume #	Crossing #	Date	Time [UT]	SC #	MLAT [°]	MLT [h]	Dist. [R_E]
P038	C209	2002/09/03	08:36	C4	−35	11.7	4.6
	C212		10:05	C4	24	12.3	4.2
P122	C711	2005/07/28	02:43	C2	−24	15.0	5.1
	C712		06:12	C3	−18	14.8	5.2
	C715		04:33	C2	27	14.4	4.7
P126	C736	2005/08/16	06:50	C3	−23	13.5	5.3
P140	C793	2006/03/06	13:00	C4	−17	0.5	4.8
P163	C896	2006/07/10	15:48	C4	−17	15.9	4.6
P169	C911	2006/08/24	18:40	C3	−26	13.6	5.2

Note. MLAT=magnetic latitude; MLT=magnetic local time; UT=universal time.

that can be unambiguously identified are selected. When observed below 1 Hz, observations are confirmed with FGM data. Rising tones are observed in only six plume events. This number is low with respect to the total number of plumes (189). Nevertheless, one should compare that number with the 30 plume events where M narrowband activity is noted because narrowband EMIC waves are seeds for rising tone emissions (Omura et al., 2010). In 20 % of those 30 plumes, one can also observe rising tones. As large rising tones, clearly identified by eyes, are not so common observed first in situ by Pickett et al. (2010), a few of them were also reported by Grison et al. (2013), we consider that coherent rising tones are a common feature of EMIC emissions in the vicinity of plasmaspheric plumes.

2.4. Rising Tone Events

Observation places of large rising tones are summarized in Table 3. When more than one rising tone is observed during a single crossing, the given location is the one corresponding to the largest absolute MLAT in each hemisphere. For two plumes the rising tones were observed in both hemisphere. All events are located at $|MLAT| > 15°$. Rising tones are observed up to 35° |MLAT| (C209). Eight of the nine crossings are located in noon-afternoon sector ([11 hr MLT ; 16 hr MLT]). Rising tone crossing occurring close to midnight (C793) is striking, as there is a kind of repetition pattern with no EMIC emissions as seed. It presents some similarity with case studied by Grison et al. (2016). Rising tone observed during crossing C736 will be analyzed in section 3.

Besides P140 and P169 that are crossed only once, rising tones are never observed in every crossings of a plume. The rising tones are observed only in one third (9/28) of the different crossings of the same plume (see Table 2). This is a highly variable process, accordingly to the localized phenomenon at the plasmapause noted by Grison et al. (2013). Three of the six plumes, P038, P122, and P126, are crossed in both hemispheres. Rising tones are observed in each hemisphere in two of these plumes.

Rising tones can be observed in a wide range of MLAT (up to 59° for P038) and in long time windows (3.5 hr for P122), in the same plume event. The low extent in MLT (0.6 hr) and radial distance (0.4 R_E) result from the orbit of the Cluster fleet. Cluster perigee and its polar orbit make the plume encounter rather unlikely close to the magnetic equatorial plane (Darrouzet et al., 2008).

Plasmaspheric plumes occurrence maximizes in the 14-17 MLT sector (see Figure 8 in Darrouzet et al., 2008). Four rising tone events are reported in that sector, four in the 11-14 MLT sector and one in the midnight sector. As 8/9 events are observed between 11 and 16 MLT, the noon-afternoon MLT sector can be seen as a preferred sector for rising tone observations. It is worth to notice that the effects of magnetosphere compression are stronger in that sector too.

Based on these results we note that EMIC rising tones, when observed, are common off the magnetic equatorial plane (above 20° MLAT). Rising tone observations above 20° MLAT are a new result of this study. Omura et al. (2010) showed that the equatorial plane region was a preferred region for EMIC rising tone triggering process. Grison et al. (2016) observed that EMIC tones triggered in the proton branch close to the magnetic equatorial plane in the plasmapause density gradient (close to midnight MLT) are reflected below 15° MLAT.

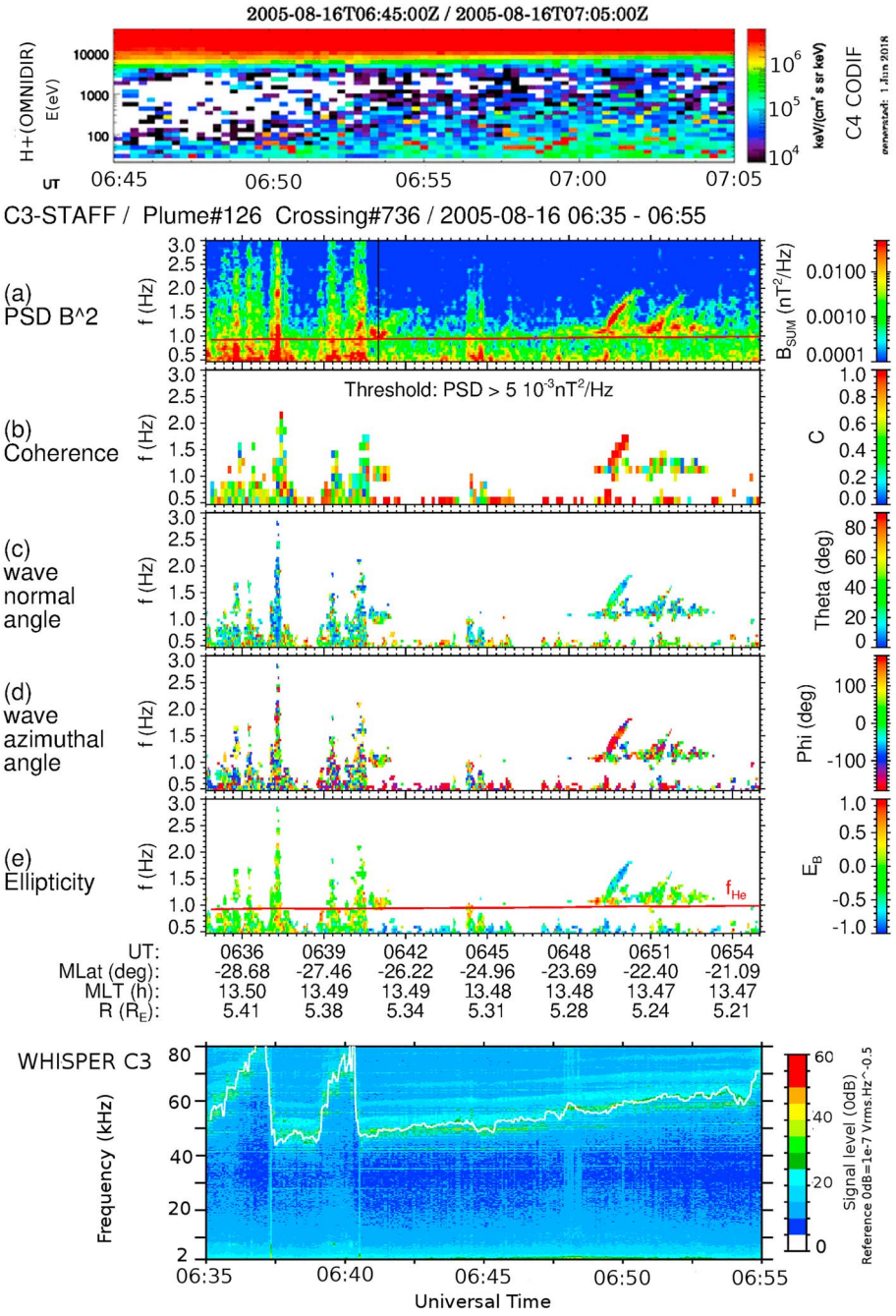

Figure 3. Wave and particle observations (16 August 2005). Top: proton energy-time spectrogram, in particle energy flux units (all directions, Cluster 4/CODIF data). Middle: wave properties (Cluster 3/STAFF-SC data): total magnetic power spectral density (a), coherence (b), wave normal angle (c), wave azimuthal angle (d), and ellipticity (e). Large rising tone is seen at 06:50 UT. Spacecraft exits the plume at 06:41 (vertical black line, panel a). The 10-min lag between wave and particle windows takes into account Cluster 3/Cluster 4 separation. Bottom: time-frequency electric field spectrogram (Waves of High frequency and Sounder for Probing of Electron density by Relaxation (WHISPER) instrument). Plasma frequency is overplotted in white. STAFF-SC and WHISPER plots have the same timescale.

Table 4
Wave Vector Inclination θ_k of the Rising Tone (Observations)

Frequency	[*Hz*]	[1.0, 1.2]	[1.2, 1.4]	[1.4, 1.6]	[1.6, 1.8]
θ_k	[°]	—	26	18	10

3. Detailed Analysis of a Crossing With Rising Tone Observations (C736)

3.1. Wave and Particle Observations

On 16 August 2005 Cluster 3 crosses a plasmaspheric plume (P126, C736) between 06:00 and 06:41 UT, based on WHISPER plasma frequency data (Darrouzet et al., 2008). Each Cluster spacecraft crossed the plume twice. A large rising tone (see detailed observations in the following paragraphs) is observed at 06:50 UT just outside the plume boundary (vertical black line, panel a of Figure 3). We checked other Cluster spacecraft PSD data: Less-intense rising tone is seen in Cluster 4 data in the same region about 1 min later. Cluster 4 is ≈3,000 km away from Cluster 3; both spacecraft follow almost the same orbit, Cluster 3 moving ahead by about 10 min.

Proton energy-time spectrogram of the particle energy flux (CIS/CODIF instrument) is presented on the top part of Figure 3. Cluster 4/CODIF instrument has the best sensibility for this event; no such observations are available on Cluster 3. An energetic ion population (energy above 5 keV) is observed during the 20-min window duration and is characteristic of the ring current (Dandouras et al., 2018). The flux intensity of the low-energy (<100 eV) population intensifies during the event. It might correspond to tail intensification of the plasmasphere population, marking the plasmasphere approach as discussed hereafter (WHISPER spectrogram on Figure 3). Between 06:50 and 07:00 (see the previously mentioned lag between Cluster 3 and 4), both ion populations are observed, which supports the hypothesis of a local tone triggering process (Omura et al., 2010). However, the ion temperature anisotropy remains low during that period. The ratio of the perpendicular to parallel temperature components is lower than 1.25 (not shown). There is also evidence of a radiation belt population, starting from 06:40 UT (data not shown).

Middle part of Figure 3 gathers wave properties obtained from STAFF-SC measurements between 06:35 and 06:55 UT, from top to bottom the total magnetic PSD (a), coherence in the polarization plane (b), wave vector inclination angle θ_k (c), wave vector azimuthal angle ϕ_k (d), and ellipticity of polarization (e). These parameters are computed in the frequency domain with the singular value decomposition method (for more details, see Santolík et al., 2002, 2003). We could not compute the Poynting flux due to bad electric field data coverage for that event.

A large rising tone is seen at 06:50 UT (Figure 3a). Its foot frequency is just above f_{He^+}, and its frequency extends of about 0.7 Hz, from 1.1 up to 1.8 Hz. The tone sweep rate is about 10^{-2} Hz·s^{-1}. The coherence of the rising tone (Figure 3b) is remarkably high, red close to 1, as compared to the coherence of emissions of a similar intensity. The wave vector is more field aligned in the highest frequency part of the tone, where blue is the dominant color, than in the lowest part, where green is the dominant color (Figure 3c and Table 4). The wave vector is earthward oriented ($\phi_k \approx \pm 180°$, Figure 3d). The tone ellipticity is clearly left handed above 1.5 Hz (blue color in Figure 3e). At its foot, EMIC wave polarization is elliptical and slightly right handed (yellowish color).

The electric field spectrogram (WHISPER instrument) is shown in the bottom part of Figure 3. The electron plasma frequency is plotted in plain white line. Two abrupt decreases are clearly seen (06:37 and 06:41 UT). The second one marks the plume exit. After 06:41, f_{pe} progressively increases, marking the plasmapause approach.

Based on the polarization and θ_k angle changes observed as a function of the frequency, we identify the tone mode as the class III in Rauch and Roux (1982) or the mode 4 in Horne and Thorne (1993): It is right-handed polarized below the crossover frequency (f_{cr}) and left handed above it. We recall that f_{cr} is above the cutoff frequency, which is above f_{He^+}. In the observed frequency range, these waves are mainly field guided. The rising tone properties, left-hand polarization, low θ_k, and high coherence level, are mostly similar to the one observed close to the triggering place (Grison et al., 2013; Omura et al., 2010; Pickett et al., 2010).

Assuming that along the field line f_{cr} normalized value ($f^*_{cr} = f_{cr}/f_{H^+}$) remains the same, the rising tone polarization would be left hand, starting from 1.1 Hz, in a region where $\mathbf{B}_0$ intensity is lower than the local one. Trigger should have occurred along the magnetic field line, considering guided propagation in a dipole magnetic field, somewhere between the observation place and the magnetic equatorial plane, where $\mathbf{B}_0$ intensity along the field line is the lowest.

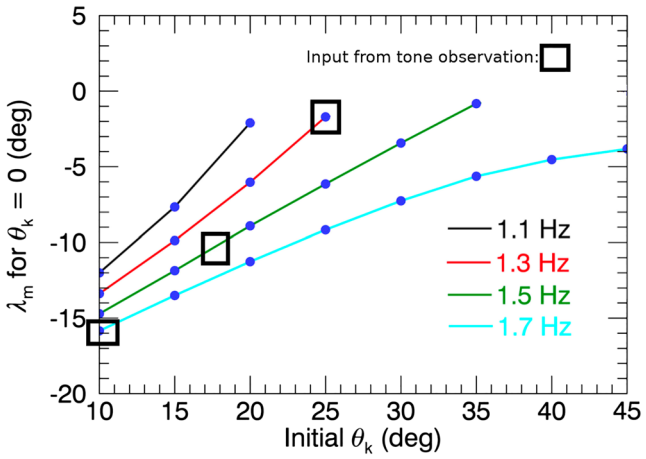

Figure 4. Results of ray tracing analysis (backward propagation) with negligible population of He^+ and O^+. Magnetic latitude (λ_m) at which the wave vector becomes parallel (or reaches the magnetic equator) is plotted with respect to the initial wave normal angle (θ_k) of the wave at $\lambda_m = -23°$. Blue dots show that the waves always stay left polarized. Only some of the lower frequency waves with very oblique initial wave normal angles reach the equator before becoming parallel. Results for the observational values are indicated by squares.

3.2. Ray Tracing Analysis

To gain more knowledge concerning the source location and propagation characteristics of the rising tone emission, we perform a ray tracing analysis in cold plasma approximation. Note that the procedure (Santolík et al., 2009) checks for the possible violation of the WKB approximation at every trajectory point, thus ensuring the validity of the results. Cold plasma density measurements are not detailed enough in the present case to reconstruct the density variation in the plasmaspheric plume. We choose to use a radial density profile based on density measurements and a diffusive equilibrium model. Additional Gaussian fits to match density measurements are performed. Radial profiles of the plume and of the plasmapause gradient are obtained from the spacecraft potential (EFW data) calibrated by WHISPER density measurements. For the sake of simplicity, Earth's magnetic field is modeled by a simple dipole.

Initial conditions for the ray tracing analysis are frequency from 1.0 to 1.9 Hz with a step of 0.1 Hz, wave normal angle from 10° to 45° with a step of 5° , MLAT $\lambda_m = -23°$, radial distance R = 5.2 R_E, and cold plasma populations, including heavy ions (5% He^+ and 10% O^+ fractions). Rays are launched from the Cluster 3 satellite position back to the equator. θ_k and ellipticity are computed along the trajectories. We assume that the polarization reversal seen on panel d of Figure 3 takes place at the local crossover frequency (≈1.0 Hz). Above this frequency, wave vectors with an initial inclination lower than 30° become parallel before the waves reach the equator. Changes in heavy ion fractions (up to 10% fraction) lead to similar results. Assuming a parallel generation for the rising tone emission (Omura et al., 2010), these waves should be generated out of the magnetic equatorial plane.

We also test emission propagation in a pure electron-proton plasma. Thus, the waves always remain left polarized. Figure 4 shows the latitudinal position of backward traced waves when the wave normal angle becomes parallel ($\theta_k = 0°$). Only cases when θ_k becomes parallel before reaching the magnetic equator are shown. Even in this extreme case with no heavy ions, none of the rays with initial θ_k below 25° reaches equator before the wave normal angle drops to 0° .

It must be noted that rays with low initial wave normal angles propagated to their assumed source with almost no dispersion, hinting at possible deficiencies in our models. We emphasize here that a more complete ray tracing analysis with realistic density, plasma composition, and magnetic field models is left for a further study. Nevertheless, our results, assuming a parallel generation assumption and a nonducted propagation, show that the observed rising tone waves are not propagating from the magnetic equatorial plane.

4. Discussion

Our study is based on the list of plasmaspheric plumes and the time intervals (±30 min before and after the plume crossing) used in Usanova et al. (2013) study. EMIC emissions are observed by Usanova et al. (2013) in 14% of these time intervals, and we observe medium intensity narrowband emissions in 6% of the plume crossings. The PSD threshold level used in our study (10^{-3} $nT^2 \cdot Hz^{-1}$) has a direct impact on the selected number of events. Other differences between these two studies are different data sets (STAFF-SC data vs. FGM data) and methodology (visual inspection vs. automatic detection). Using STAFF-SC data instead of FGM data provides a better coverage of the H^+ band and a worse coverage of the He^+ band. This also contributes to the lower occurrence rate found in our study, as narrowband EMIC emissions are more frequent in the He^+ band than in the H^+ and O^+ bands (Saikin et al., 2015). Conclusions remain unchanged: Plasmaspheric plumes and their vicinity are not a preferred region for observations of narrowband emissions below local proton gyrofrequency.

It is uncommon to observe narrow band emissions and/or rising tones in more than one third of the crossings of the same plume (60/175 and 9/28, respectively) as can be seen in Table 2. Narrowband emissions and rising tones are localized in space and time at lower scales than the characteristic plume scale. Broadband emissions are commonly observed in the inner magnetosphere region (Chaston et al., 2015). It is not surprising to observed them also in the vicinity of plumes.

None of the present rising tones (cf. Table 3) are reported in the Cluster survey of Grison et al. (2013). This survey was performed using a visual inspection of single component spectrograms (http://cluster.lpp.polytechnique.fr/staff/N2nbr/main2018.html). Looking afterward again at these spectrograms, no rising tones could be visually identified. Reasons are the different spectrogram dynamic scales and the weak PSD of the rising tone along the component chosen for the spectrogram (along the spin axis).

Considering the degree of polarization and the frequency dispersion, Nakamura et al. (2016) reported a larger occurrence of rising tones (reported in 30% of the EMIC events) in the magnetosphere than in the present study, limited to the plasmaspheric plumes. The equatorial orbit of the Time History of Events and Macroscale Interactions during Substorms (THEMIS) spacecraft can explain to a large extent this occurrence rate difference, as the most favorable local conditions for triggering process are found close to the magnetic equatorial plane, and not only in the vicinity of plasmaspheric plumes. However, this higher occurrence rate might also be explained by the automatic detection method used in that study, which might be more powerful than visual inspection, and by the criterion on the coherence considered in our study, which is more selective than a criterion on the degree of polarization.

An EMIC rising tone generated in the proton branch close to the magnetic equatorial plane is reflected toward the magnetic equator at 15° MLAT as reported by Grison et al. (2016). We report rising tone observations at absolute MLATs larger than 20° . Wave and particle properties, and preliminary ray tracing analysis, indicate that a propagation of such a rising tone (cf. section 3) from the magnetic equator is unlikely. We thus believe that rising tones can be triggered at MLATs above 15° . Nonlinear process consecutive to saturation of EMIC linear wave growth is more probable in a place where intense EMIC waves are observed. The triggering region of the rising tones might thus be related to secondary EMIC source region that was found above 15° MLAT (Allen et al., 2016). This region related to particles executing Shabansky orbits is mainly found at higher L-shells (8 to 10), where $\mathbf{B}_0$ is locally depressed, than the rising tone location. However, McCollough et al. (2012) underlined the potential role of plasmaspheric plumes for EMIC growth in this source region.

5. Conclusion

Starting with 935 plume crossings reduced to 189 unique plumes, we compare the occurrence rates of broadband, narrowband, and rising tones emissions close to plasmaspheric plumes in the [1-10] Hz frequency range. In time intervals starting 30 min before the plume entry and lasting 30 min after the plume exit, broadband emissions are the most common emissions (observed in 67% of the 189 plumes), followed by narrowband emissions (in 16%) and EMIC rising tones (in 3%).

Broadband emissions are not specifically related to plasmaspheric plume, as they are commonly observed everywhere in the inner magnetosphere region (Chaston et al., 2015). Based on different data set and methodology we confirm results of Usanova et al. (2013) that the plumes are not a preferred place for narrowband emissions. EMIC rising tones are observed in 20% of the 30 plumes when narrowband emissions are also observed. Tone identification results from a clear frequency dispersion *and* a large coherence value. As compared to a few previously reported cases matching these two criteria (Grison et al., 2013; Pickett et al., 2010), plumes and their vicinity appear as a common place for observing EMIC rising tones. We plan to perform in the future an automatic detection of rising tones based on these criteria to confirm that result. The presence of energetic ions associated to a dense cold population and a density gradient can explain the larger occurrence of the non linear stage of EMIC wave growth, allowing rising tone generation.

Nine new rising tone events are found at absolute MLATs larger than 17° and for eight of them in the 11–17 MLT sector. Based on wave properties and preliminary ray tracing analysis performed in a detailed case study, tone propagation from the magnetic equator to the observation place is rather unlikely. We presume that the rising tone generation can take place at MLATs above 15°, as this region is known to be a source region for EMIC waves (Allen et al., 2016). This might have implication for particle precipitations enhanced by large EMIC rising tones (Shoji & Omura, 2012).

Acknowledgments
The list of plume is available upon request (contact Fabien.Darrouzet@aeronomie.be). We acknowledge support of GACR Grant 18-05285S, of the the Mobility Plus grant JSPS-17-14, and of the Praemium Academiae Award from the Czech Academy of Sciences. Cluster data are publicly available through the Cluster Science Archive (CSA, https://www.cosmos.esa.int/web/csa). We acknowledge FGM and WHISPER teams and CSA for supplying Cluster data. The work of F. D. was supported by the Prodex project (contract 13127/98/NL/VJ). We thank V. Mašatová for her involvement in the preliminary stage of the study.

References

Allen, R. C., Zhang, J.-C., Kistler, L. M., Spence, H. E., Lin, R.-L., Klecker, B., et al. (2016). A statistical study of EMIC waves observed by Cluster: 2. Associated plasma conditions. *Journal of Geophysical Research: Space Physics*, *121*, 6458–6479. https://doi.org/10.1002/2016JA022541

Anderson, B. J., Erlandson, R. E., & Zanetti, L. J. (1992). A statistical study of Pc 1-2 magnetic pulsations in the equatorial magnetosphere. I - equatorial occurrence distributions, II - wave properties. *Journal of Geophysical Research*, *97*, 3075–3101. https://doi.org/10.1029/91JA02706

Balogh, A., Carr, C. M., Acuña, M. H., Dunlop, M. W., Beek, T. J., Brown, P., et al. (2001). The Cluster magnetic field investigation: Overview of in-flight performance and initial results. *Annales Geophysicae*, *19*(10), 1207–1217. https://doi.org/10.5194/angeo-19-1207-2001

Chaston, C. C., Bonnell, J. W., Kletzing, C. A., Hospodarsky, G. B., Wygant, J. R., & Smith, C. W. (2015). Broadband low-frequency electromagnetic waves in the inner magnetosphere. *Journal of Geophysical Research: Space Physics*, *120*, 8603–8615. https://doi.org/10.1002/2015JA021690

Cornilleau-Wehrlin, N., Chanteur, G., Perraut, S., Rezeau, L., Robert, P., Roux, A., et al. (2003). First results obtained by the Cluster STAFF experiment. *Annales Geophysicae*, *21*(2), 437–456. https://doi.org/10.5194/angeo-21-437-2003

Dandouras, I., Rochel-Grimald, S., Vallat, C., & Dunlop, M. W. (2018). Terrestrial ring current. In A. Keiling, O. Marghitu, & M. Wheatland (Eds.), *Electric Currents in Geospace and Beyond*. https://doi.org/10.1002/9781119324522.ch7

Darrouzet, F., De Keyser, J., Décréau, P. M. E., El Lemdani-Mazouz, F., & Vallières, X. (2008). Statistical analysis of plasmaspheric plumes with Cluster/WHISPER observations. *Annales Geophysicae*, *26*(8), 2403–2417. https://doi.org/10.5194/angeo-26-2403-2008

Darrouzet, F., Gallagher, D. L., André, N., Carpenter, D. L., Dandouras, I., Décréau, P. M. E., et al. (2009). Plasmaspheric density structures and dynamics: Properties observed by the CLUSTER and IMAGE missions. *Space Science Review*, *145*, 55–106. https://doi.org/10.1007/s11214-008-9438-9

Décréau, P. M. E., Fergeau, P., Krasnoselskikh, V., Le Guirriec, E., Lévêque, M., Martin, P., et al. (2001). Early results from the WHISPER instrument on Cluster: An overview. *Annales Geophysicae*, *19*(10/12), 1241–1258. https://doi.org/10.5194/angeo-19-1241-2001

Elphic, R. C., Weiss, L. A., Thomsen, M. F., McComas, D. J., & Moldwin, M. B. (1996). Evolution of plasmaspheric ions at geosynchronous orbit during times of high geomagnetic activity. *Geophysical Research Letters*, *23*(16), 2189–2192. https://doi.org/10.1029/96GL02085

Escoubet, C. P., Fehringer, M., & Goldstein, M. (2001). The Cluster mission. *Annales Geophysicae*, *19*(10/12), 1197–1200. https://doi.org/10.5194/angeo-19-1197-2001

Grison, B., Darrouzet, F., Santolík, O., Cornilleau-Wehrlin, N., & Masson, A. (2016). Cluster observations of reflected EMIC-triggered emission. *Geophysical Research Letters*, *43*, 4164–4171. https://doi.org/10.1002/2016GL069096

Grison, B., Santolík, O., Cornilleau-Wehrlin, N., Masson, A., Engebretson, M. J., Pickett, J. S., et al. (2013). EMIC triggered chorus emissions in Cluster data. *Journal of Geophysical Research: Space Physics*, *118*, 1159–1169. https://doi.org/10.1002/jgra.50178

Gustafsson, G., André, M., Carozzi, T., Eriksson, A. I., Fälthammar, C.-G., Grard, R., et al. (2001). First results of electric field and density observations by Cluster EFW based on initial months of operation. *Annales Geophysicae*, *19*(10), 1219–1240. https://doi.org/10.5194/angeo-19-1219-2001

Horne, R. B., & Thorne, R. M. (1993). On the preferred source location for the convective amplification of ion cyclotron waves. *Journal of Geophysical Research*, *98*(A6), 9233–9247. https://doi.org/10.1029/92JA02972

Kennel, C. F., & Petschek, H. E. (1966). Limit on stably trapped particle fluxes. *Journal of Geophysical Research*, *71*, 1. https://doi.org/10.1029/JZ071i001p00001

McCollough, J. P., Elkington, S. R., & Baker, D. N. (2012). The role of Shabansky orbits in compression-related electromagnetic ion cyclotron wave growth. *Journal of Geophysical Research*, *117*, A01208. https://doi.org/10.1029/2011JA016948

Nakamura, S., Omura, Y., & Angelopoulos, V. (2016). A statistical study of EMIC rising and falling tone emissions observed by THEMIS. *Journal of Geophysical Research: Space Physics*, *121*, 8374–8391. https://doi.org/10.1002/2016JA022353

Nykyri, K., Grison, B., Cargill, P. J., Lavraud, B., Lucek, E., Dandouras, I., et al. (2006). Origin of the turbulent spectra in the high-altitude cusp: Cluster spacecraft observations. *Annales Geophysicae*, *24*(3), 1057–1075. https://doi.org/10.5194/angeo-24-1057-2006

Omura, Y., Pickett, J., Grison, B., Santolik, O., Dandouras, I., Engebretson, M., et al. (2010). Theory and observation of electromagnetic ion cyclotron triggered emissions in the magnetosphere. *Journal of Geophysical Research*, *115*, A07234. https://doi.org/10.1029/2010JA015300

Pickett, J. S., Grison, B., Omura, Y., Engebretson, M. J., Dandouras, I., Masson, A., et al. (2010). Cluster observations of EMIC triggered emissions in association with Pc1 waves near Earth's plasmapause. *Geophysical Research Letters*, *37*, L09104. https://doi.org/10.1029/2010GL042648

Rauch, J. L., & Roux, A. (1982). Ray tracing of ulf waves in a multicomponent magnetospheric plasma: Consequences for the generation mechanism of ion cyclotron waves. *Journal of Geophysical Research*, *87*(A10), 8191–8198. https://doi.org/10.1029/JA087iA10p08191

Rème, H., Aoustin, C., Bosqued, J. M., Dandouras, I., Lavraud, B., Sauvaud, J. A., et al. (2001). First multispacecraft ion measurements in and near the Earth's magnetosphere with the identical Cluster ion spectrometry (CIS) experiment. *Annales Geophysicae*, *19*(10/12), 1303–1354. https://doi.org/10.5194/angeo-19-1303-2001

Robert, P., Cornilleau-Wehrlin, N., Piberne, R., de Conchy, Y., Lacombe, C., Bouzid, V., et al. (2014). CLUSTER-STAFF search coil magnetometer calibration-comparisons with FGM. *Geoscientific Instrumentation, Methods and Data Systems*, *3*(2), 153–177. https://doi.org/10.5194/gi-3-153-2014

Saikin, A. A., Zhang, J., Allen, R. C., Smith, C. W., Kistler, L. M., Spence, H. E., et al. (2015). The occurrence and wave properties of H^+-, He^+-, and O^+-band EMIC waves observed by the Van Allen Probes. *Journal of Geophysical Research: Space Physics*, *120*, 7477–7492. https://doi.org/10.1002/2015JA021358

Santolík, O., Parrot, M., Inan, U. S., Burešová, D., Gurnett, D. A., & Chum, J. (2009). Propagation of unducted whistlers from their source lightning: A case study. *Journal of Geophysical Research*, *114*, A03212. https://doi.org/10.1029/2008JA013776

Santolík, O., Parrot, M., & Lefeuvre, F. (2003). Singular value decomposition methods for wave propagation analysis. *Radio Science*, *38*(1), 1010. https://doi.org/10.1029/2000RS002523

Santolík, O., Pickett, J. S., Gurnett, D. A., & Storey, L. R. O. (2002). Magnetic component of narrowband ion cyclotron waves in the auroral zone. *Journal of Geophysical Research*, *107*, 1444. https://doi.org/10.1029/2001JA000146

Shoji, M., & Omura, Y. (2012). Precipitation of highly energetic protons by helium 1 branch electromagnetic ion cyclotron triggered emissions. *Journal of Geophysical Research*, *117*, A12210. https://doi.org/10.1029/2012JA017933

Usanova, M. E., Darrouzet, F., Mann, I. R., & Bortnik, J. (2013). Statistical analysis of EMIC waves in plasmaspheric plumes from Cluster observations. *Journal of Geophysical Research: Space Physics*, *118*, 4946–4951. https://doi.org/10.1002/jgra.50464

Usanova, M. E., Mann, I. R., Bortnik, J., Shao, L., & Angelopoulos, V. (2012). THEMIS observations of EMIC wave occurrence: Dependence on AE, SYMH, and solar wind dynamic pressure. *Journal of Geophysical Research*, *117*, A10218. https://doi.org/10.1029/2012JA018049